Clean Technol., Vol. 30, No. 3, September 2024, pp. 267-275

청정에너지기술 보 문

Hierarchical SnO_2 Nanoflakes Integrated with Carbon Nanofibers as an Advanced Anode Material for High-Performance Lithium-Ion Batteries

Ying Liu[1,2†], Jungwon Heo[1†], Dong-Ho Baek[1], Dengzhou Liu[3], Dirfan Zabrian[3], Mingxu Li[3], Prasanth Raghavan[4], Jae-Kwang Kim[2]*, and Jou-Hyeon Ahn[1,3]*

[1]Department of Chemical Engineering, Gyeongsang National University
Jinju 52828, Republic of Korea
[2]Department of Energy Convergence Engineering, Cheongju University
285 Daseong-ro, Cheongju 28503, Republic of Korea
[3]Department of Materials Engineering and Convergence Technology, Gyeongsang National University
Jinju 52828, Republic of Korea
[4]Department of Polymer Science and Rubber Technology, Cochin University of Science and Technology
Kochi, 682022, India

(Received for review July 4, 2024; Revision received August 8, 2024; Accepted August 9, 2024)

Abstract

Lithium-ion batteries (LIBs) have attracted significant attention as potential energy storage solutions due to their high energy density, minimal self-discharge, extended cycle life, and absence of memory effects. However, conventional LIBs use graphite as the anode material and as a result struggle to meet the increasing demand for higher energy density because of the low theoretical capacity of graphite. In order to enhance Li storage capacity and address the current limitations of LIBs, this study designed and analyzed SnO_2 nanoflakes/CNF, which is an advanced anode material with a unique hierarchical structure synthesized via a facile method involving incipient wetness followed by annealing. The *in-situ* formed SnO_2 nanoflakes improve the electrolyte accessibility and shorten the ion and electron transport pathways, thereby enhancing the reaction kinetics. Additionally, the CNF matrix enhances the electrical conductivity, accelerates electron transport, and mitigates volume changes. The integrated SnO_2 nanoflakes/CNF cell demonstrated outstanding cycling performance and excellent rate capability, achieving a notable reversible capacity of 636 mAh g^{-1} after 100 cycles at 0.1 C. This study provides valuable insights into the design of high-efficiency anode materials for the advancement of high-performance LIBs.

Keywords : Hierarchical structure, SnO_2 nanoflakes, Carbon nanofiber, Anode, Rechargeable Li-SnO_2 batteries

1. Introduction

Lithium-ion batteries (LIBs) with high energy density and extended lifespans are essential for addressing the increasing energy storage requirements of electric vehicles, smart grids, and other energy storage systems[1-3]. Graphite, the standard anode material in LIBs, struggles to meet the rising demand for higher energy density due to its low theoretical capacity (372 mAh g^{-1})[4,5]. Thus, developing advanced anode materials with higher theoretical capacities is essential to surpass the current limitations of LIBs. Transition–metal oxides (TMOs) have emerged as promising alternatives to graphite owing to their rich in natural resources and outstanding Li storage capacity[6-8]. Among TMOs, SnO_2 is notable as an anode material for lithium storage due to its high theoretical capacity, non-toxicity, and cost-effectiveness. However, SnO_2 undergoes significant volumetric changes (>300%) during charge-discharge cycles, leading to rapid capacity degradation, poor cycling performance, and inferior rate capability[9,10].

To tackle these challenges, a synergistic approach that integrates tailored SnO_2 nanoparticles with carbon matrices has been shown to effectively enhance the electrochemical performance of rechargeable Li-SnO_2 batteries. The tailored SnO_2 nanoparticles, with their unique structure, can shorten ion transport pathways and improve electrolyte accessibility, thereby facilitating reaction

†These two authors contributed equally to this work.
*To whom correspondence should be addressed.
E-mail: jaekwang@cju.ac.kr, Tel: +82-43-883-4788
E-mail: jhahn@gnu.ac.kr, Tel, +82-55-772-1784, Fax: +82-55-772-1789
https://doi.org/10.7464/ksct.2024.30.3.267 pISSN 1598-9712 eISSN 2288-0690

kinetics. The carbon matrices, characterized by high electrical conductivity, enhance electron transport and buffer volume changes, further improving electrochemical performance. For example, Lu et al.[11] reported three-dimensional reduced graphene oxide-encapsulated SnO_2 nanoparticles, achieving a remarkable capacity retention of 1,592 mAh g^{-1} over 500 cycles at 0.5 A g^{-1}. Similarly, Wang et al.[12] synthesized a $Sn/SnO_2/C$ nanohybrid, where ultrafine SnO_2/Sn nanoparticles encapsulated within an adjustable mesoporous carbon matrix maintained a high-capacity retention of 1,105 mAh g^{-1} at 200 mA g^{-1} after 290 cycles. Undoubtedly, the rational design of SnO_2 with a unique structure integrated with a carbon matrix can significantly enhance the cycling performance and rate capability of rechargeable Li-SnO_2 batteries owing to the synergistic effect between the components.

Hence, we have elaborately designed a hierarchical structure in which SnO_2 nanoflakes are integrated within carbon nanofibers (CNF) using a facile incipient wetness technique followed by an annealing process, effectively address challenges associated with rechargeable Li-SnO_2 batteries. The CNF matrix plays a significant role in increasing conductivity, accelerating electron transport, and alleviating volume changes. Meanwhile, the *in-situ* formed SnO_2 nanoflakes reduce pathways for ion and electron transport, thereby enhancing reaction kinetics. Consequently, the unique hierarchical structure of the SnO_2 nanoflakes/CNF anode material demonstrates exceptional cycling performance and rate capability, achieving a remarkable lithiation capacity retention of 636 mAh g^{-1} at 0.1 C after 100 cycles. This hierarchical SnO_2 nanoflakes/CNF composite shows outstanding rate performance and cycling stability, making it an excellent candidate for advanced LIB anodes.

2. Materials and methods

2.1 Materials

Polyacrylonitrile (PAN, average MW 150,000, Sigma-Aldrich), N, N-dimethylformamide (DMF, 99.0%, Samchun Pure Chemical Co., Ltd.), tin (II) chloride dihydrate ($SnCl_2{\cdot}2H_2O$, 98.0%, Sigma-Aldrich), Tin oxalate ($Sn(C_2O_4)$, 98.0%, Sigma-Aldrich), hexamethylenetetramine (HMTA, 99.0%, Samchun Pure Chemical Co., Ltd.), thiourea (SCN_2H_4, 98.0%, Samchun Pure Chemical Co., Ltd.), ethylene glycol (99.8%, Sigma-Aldrich), Tin oxide nanopowder (Sigma-Aldrich), and N-methylpyrrolidone (NMP, 99.5%, Samchun Pure Chemical Co., Ltd.) were used as received.

2.2 Preparation of SnO_2 nanoflakes/CNF and SnO_2 nanoflakes composites

To synthesize SnO_2 nanoflakes/CNF composite, a series of steps were followed, beginning with the preparation of CNF using a straightforward electrospinning method. Initially, PAN was dissolved in DMF at 60 °C for 12 h with continuous stirring. The PAN solution was then loaded into a syringe fitted with a 21-gauge metallic needle. Electrospinning was performed by applying a high voltage of 17 kV at a flow rate of 3 mL h^{-1}, with the collector placed 18 cm from the needle. The resulting PAN fibers were stabilized at 300 °C for 3 h in an air atmosphere and then carbonized at 800 °C for 5 h with a heating rate of 3 °C min^{-1} under an Ar atmosphere. Simultaneously, a solution of $Sn(C_2O_4)$ and HMTA in an equal molar ratio was prepared by dissolving the compounds in 500 mL of distilled water to achieve a concentration of approximately 0.05 M, forming a white milky solution. The CNF was immersed in this solution and heated at 150 °C for 1 h. After washing, the mixture was calcinated at 350 °C for 3 h in an air atmosphere, resulting in the formation of SnO_2 nanoflakes/CNF composite.

For a thorough comparison of electrochemical performance, SnO_2 nanoflakes were also synthesized according to a previously reported method[13]. A 0.05 M solution of $SnCl_2{\cdot}2H_2O$ and a 0.1 M solution of thiourea were added to 100 mL of ethylene glycol in a round-bottom flask and heated at 170 °C for 1 h. After washing, the mixture was calcinated at 500 °C for 3 h in an air atmosphere, resulting in the formation of SnO_2 nanoflakes.

2.3 Characterization of materials

The external morphologies of the synthesized samples were observed using field-emission scanning electron microscopy (FE-SEM, TESCAN, MIRA3 LM), while their internal structures were investigated by transmission electron microscopy (TEM, FEI, TF30ST). The crystal structures of the samples were examined using X-ray diffraction (XRD, Bruker, D2 Phaser) with Cu Kα radiation over a range of 20 ~ 80°. The specific surface area was determined through Brunauer-Emmet-Teller analysis (BET, Micromeritics, ASAP 2010). To quantify the SnO_2 content in the SnO_2 nanoflakes/CNF composite, thermogravimetric analysis (TGA, TA Instruments, Q50) was performed from room temperature to 650 °C at a heating rate of 10 °C min^{-1} in an O_2 atmosphere.

2.4 Electrochemical characterization

The anode electrodes were fabricated by mixing 80% active material (SnO_2 nanoflakes/CNF, SnO_2 nanoflakes, SnO_2 nanoparticles), 10% Super P, and 10% poly(vinylidene fluoride) (PVDF) in N-methyl-2-pyrrolidone (NMP). The homogeneous slurry was then uniformly coated onto copper foil, dried at 80 °C for 12 h under vacuum conditions, and subsequently punched into discs with a diameter of 10 mm. Lithium metal foil served as the counter electrode, Celgard® 2400 as the separator, and a 1 M lithium hexafluorophosphate ($LiPF_6$) dissolved in a mixture

of ethylene carbonate (EC) and diethylene carbonate (DEC) with a 1:1 volume ratio as the electrolyte. Galvanostatic charge/discharge testing was performed at varying current densities within a voltage range of 0.01 ~ 3.0 V using a WBCS3000 battery cycler (WonA Tech. Co., Ltd., South Korea). Cyclic voltammetry (CV) measurements were conducted at a scan rate of 0.5 mV s^{-1}. Electrochemical impedance spectroscopy (EIS) was carried out with an impedance analyzer (ZIVE SP2, WonA Tech. Co., Ltd.) over a frequency range of 0.1 Hz to 100 kHz.

3. Results and discussion

Figure 1 illustrates the preparation process of SnO_2 nanoflakes on CNF. Through a facile annealing procedure, interlaced SnO_2 nanoflakes were uniformly grown on the CNF. The resulting SnO_2 nanoflakes/CNF composite exhibits a well-dispersed fibrous structure with widths ranging from 400 to 500 nm, as depicted in Figure 2a. Moreover, the interlaced SnO_2 nanoflakes possess a thickness of approximately 10 nm. Further investigation of the microstructure of the SnO_2 nanoflakes/CNF was conducted using TEM analysis, shown in Figure 2b. The TEM image confirms that the interlaced SnO_2 nanoflakes are densely anchored on the CNF, consistent with the SEM observation. Additionally, the TEM image reveals the presence of prominent carbon within the interstices of the interlaced SnO_2 nanoflakes. This prominent carbon substantially enhances electrical conductivity and effectively buffers the volume changes during the lithiation and delithiation processes. In comparison, the morphologies of the synthesized SnO_2 nanoflakes and commercial SnO_2 nanoparticles are depicted in Figure 2(c ~ e). The SnO_2 nanoflakes exhibit similar interlaced nanoflake morphological characteristics to those of SnO_2 nanoflakes/CNF, as shown in Figure 2c. In contrast, individual SnO_2 nanoparticles display sphericity with diameters ranging from 10 to 100 nm (Figure 2d), and these nanoparticles tend to agglomerate into a bulk morphology (Figure 2e). The surface morphological and internal structural analysis reveal that the synthesized SnO_2 nanoflakes/CNF

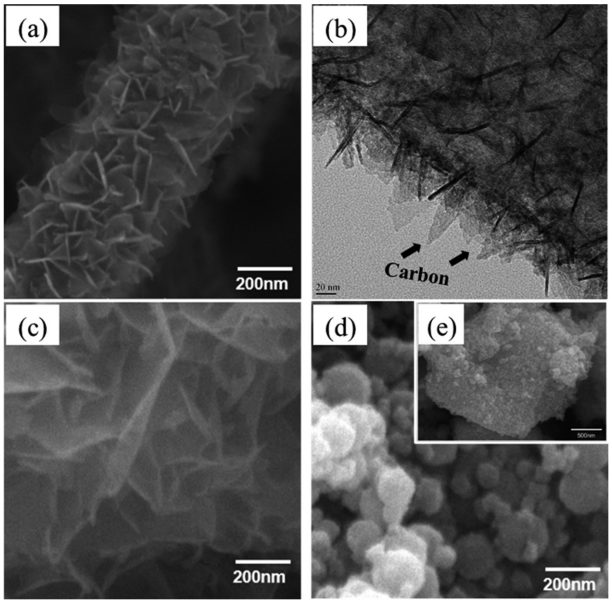

Figure 2. (a) FE-SEM image of SnO_2 nanoflakes/CNF, (b) TEM image of SnO_2 nanoflakes/CNF, FE-SEM images of (c) SnO_2 nanoflakes, and (d ~ e) SnO_2 nanoparticles.

composite features a unique hierarchical structure. The CNF acts as a supporting matrix, greatly improving electrical conductivity and preventing the agglomeration of the SnO_2 nanoflakes generated in situ. Additionally, the interlaced SnO_2 nanoflakes formed in situ enhance electrolyte accessibility and increase active sites, accelerating the reaction kinetics.

The XRD analysis presented in Figure 3a facilitated the identification of the phases in SnO_2 nanoflakes/CNF, SnO_2 nanoflakes, and SnO_2 nanoparticles. The main diffraction peaks at 26.6°, 33.2°, 37.2°, 50.7°, 60.6°, and 63.5° for SnO_2 nanoflakes/CNF corresponded precisely to the (110), (101), (200), (211), (310), and (301) crystal planes, respectively, which showed a high match with SnO_2 nanoflakes and SnO_2 nanoparticles, affirming the successful synthesis of SnO_2 in the SnO_2 nanoflakes/CNF composite[14,15]. Additionally, two distinct peaks at 29.1° and 35.7° were observed, corresponding to the (101) and (002) planes of SnO (JCPDS No. 06-0395). The presence of SnO is likely attributable to the thermal

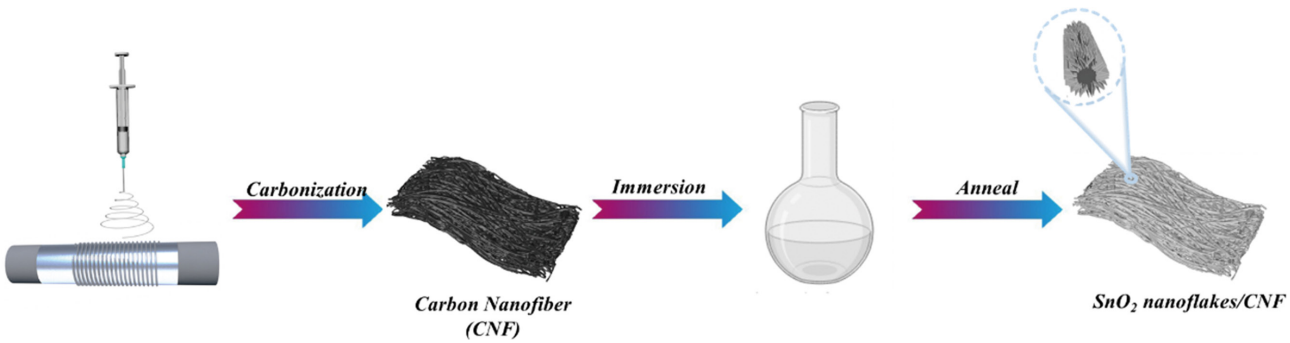

Figure 1. Illustration of the sequential fabrication steps for SnO_2 nanoflakes/CNF composite.

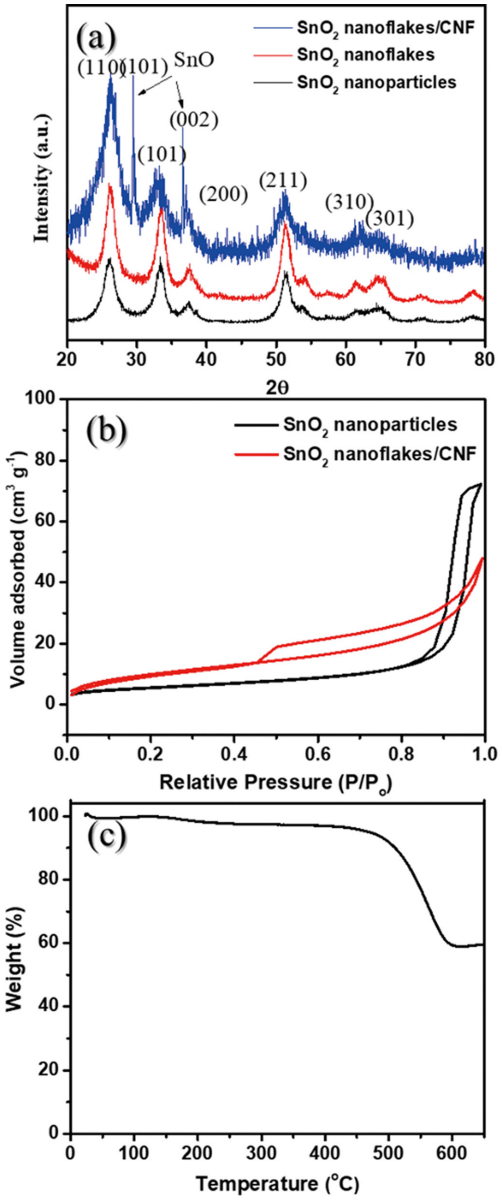

Figure 3. (a) XRD patterns of SnO_2 nanoparticles, SnO_2 nanoflakes, and SnO_2 nanoflakes/CNF, (b) nitrogen adsorption-desorption isotherms of SnO_2 nanoparticles, and SnO_2 nanoflakes/CNF, (c) TGA plot of SnO_2 nanoflakes/CNF composite.

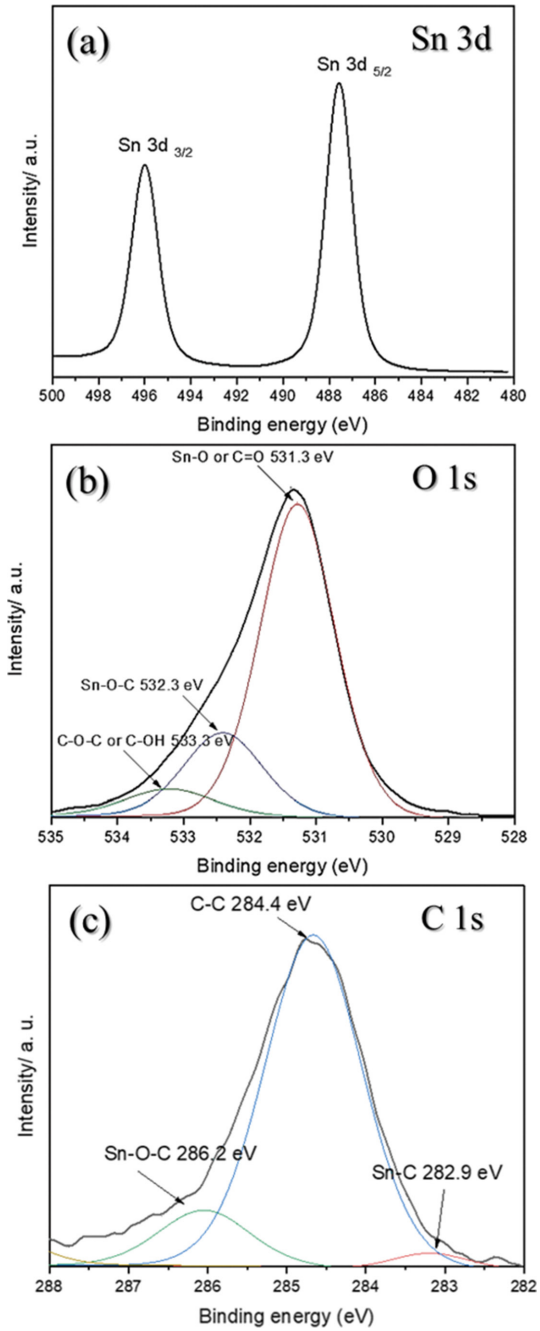

Figure 4. High-resolution (a) Sn 3d, (b) O 1s, and (c) C 1s XPS data of SnO_2 nanoflakes/CNF, respectively.

decomposition of SnC_2O_4[16]. The N_2 adsorption/desorption isotherms for SnO_2 nanoflakes/CNF and SnO_2 nanoparticles are illustrated in Figure 3b. The SnO_2 nanoflakes/CNF displayed a typical type IV isotherm with an H1-type hysteresis loop. Conversely, the SnO_2 nanoparticles exhibited a combination of type II and type IV isotherms with an H3-type hysteresis loop. The surface area of SnO_2 nanoflakes/CNF (40 m^2 g^{-1}) was larger than that of the SnO_2 nanoparticles (18 m^2 g^{-1}), indicating that SnO_2 nanoflakes/CNF is more conducive to reactions due to enhanced electrolyte accessibility. To accurately determine the SnO_2 content in the SnO_2 nanoflakes/CNF composite, TGA was conducted in an O_2 atmosphere from room temperature to 650 °C at a heating rate of 10 °C min^{-1} (Figure 3c). A substantial mass loss occurred between 450 and 550 °C, attributed to the oxidation of carbon within the SnO_2 nanoflakes/CNF composite[17]. Consequently, the SnO_2 content in the composite was estimated to be approximately 60 wt%.

The chemical properties of the SnO_2 nanoflakes/CNF composite were examined through XPS analysis (Figure 4a ~ c). The high-resolution Sn 3d spectrum of the SnO_2 nanoflakes/CNF composite reveals distinct peaks at 487.6 eV and 496.1 eV, corresponding to

Sn $3d_{5/2}$ and Sn $3d_{3/2}$, respectively. The O 1s XPS spectrum for the composite shows three peaks at 531.3 eV, 532.3 eV, and 533.3 eV, attributable to Sn-O/C=O, Sn-O-C, and C-O-C/C-OH, respectively [18-20]. Furthermore, the C 1s spectrum exhibits peaks at 282.9 eV and 286.2 eV, indicative of the formation of Sn-C and Sn-O-C bonds[21-23]. This evidence points to robust chemical bonding at the interface between SnO_2 and CNF. The presence of Sn-C and Sn-O-C interfacial bonds not only firmly anchors the SnO_2 nanoflakes to the CNF matrix but also significantly enhances the interaction between the two components[24].

The reaction mechanisms of SnO_2 nanoflakes/CNF, SnO_2 nanoflakes, and SnO_2 nanoparticles cells are investigated using the CV curves depicted in Figure 5(a ~ c). SnO_2 nanoflakes and SnO_2 nanoparticles cells exhibit similar electrochemical behaviors. During the initial cathodic scan, a voltage hysteresis around 0.5 V

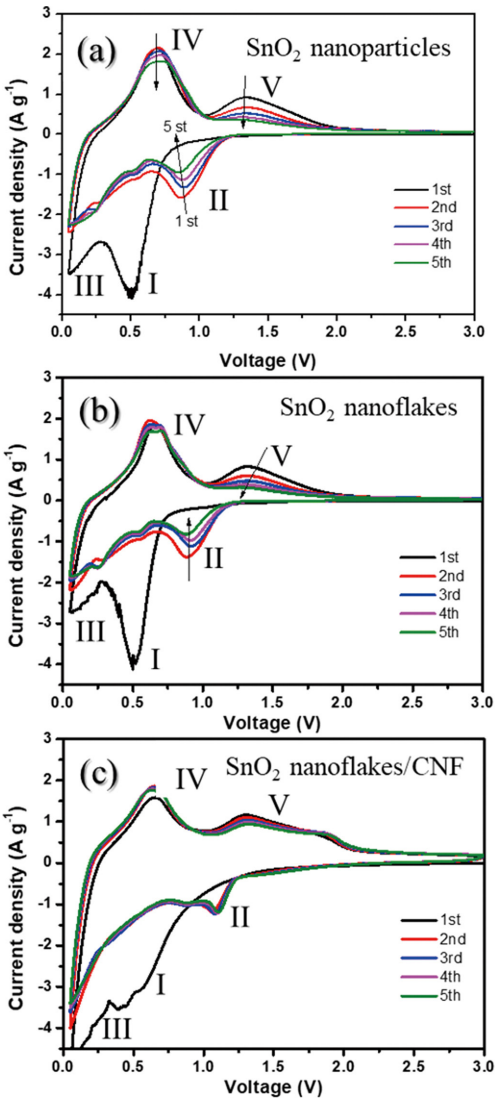

Figure 5. CV curves of (a) SnO_2 nanoparticles, (b) SnO_2 nanoflakes, (c) SnO_2 nanoflakes/CNF (scan rate: 0.5 mV s^{-1}; 0.01 ~ 3.0 V).

(Peak I) is observed, which is associated with the formation of a solid electrolyte interface (SEI) film and the irreversible decomposition of the electrolyte[25,26]. Interestingly, the current values at Peak I are significantly higher for the SnO_2 nanoflakes and SnO_2 nanoparticles cells compared to SnO_2 nanoflakes/CNF, indicating more extensive irreversible reactions in the former. This suggests that the well-engineered structure of SnO_2 nanoflakes/CNF effectively minimizes irreversible reactions during the initial lithiation process, thereby enhancing initial Coulombic efficiency and active material utilization[27]. In subsequent cycles, the lithiation voltage from Peak I shifts to Peak II, corresponding to the reduction of SnO_2 to Sn (Equation (1)). Another lithiation voltage (Peak III) is related to the alloying reaction from Sn to Li-Sn alloy (Equation (2)). The anodic peaks (Peak IV and Peak V) indicate the oxidation of Li-Sn back to Sn, and further oxidation to SnO_2[28,29]. The current value at Peak III for SnO_2 nanoflakes/CNF exceeds that of SnO_2 nanoflakes and SnO_2 nanoparticles, suggesting a more complete alloying reaction. Additionally, Peaks II, III, IV, and V for SnO_2 nanoflakes/CNF show consistent repeatability in the CV curves, reflecting a stable reaction environment. In contrast, the same peaks for SnO_2 nanoflakes and SnO_2 nanoparticles cells exhibit a continuous decline, indicating an unstable reaction environment. This stability highlights the advantages of the SnO_2 nanoflakes/CNF structure in ensuring reliable and reproducible electrochemical processes.

$$SnO_2 + 4Li^+ + 4e^- \leftrightarrow Sn + 2Li_2O \quad (1)$$

$$Sn + xLi^+ + xe^- \leftrightarrow Li_xSn (0 \le x \le 4.4) \quad (2)$$

The initial charge-discharge profiles of SnO_2 nanoflakes/CNF, SnO_2 nanoflakes, and SnO_2 nanoparticles cells at 0.1 C are shown in Figure 6a. The SnO_2 nanoflakes/CNF composite exhibited the highest lithiation capacity of 1,800 mAh g^{-1}, followed by SnO_2 nanoflakes of 1,470 mAh g^{-1}, and SnO_2 nanoparticles of 1,270 mAh g^{-1}. This indicates that the SnO_2 in the SnO_2 nanoflakes/CNF composite demonstrates the highest utilization, attributed to the synergistic effect between SnO_2 nanoflakes and CNF. In the subsequent charge-discharge profiles of SnO_2 nanoflakes (Figure 6b), capacity degradation occurred due to severe volume changes during the lithiation-delithiation processes. Conversely, from the 2nd cycle onward, the charge-discharge profiles of the SnO_2 nanoflakes/CNF cell (Figure 6c) maintained excellent repeatability, indicating that the SnO_2 nanoflakes/CNF cell possesses superior repeatability and cyclability. The cycling performance of SnO_2 nanoflakes/CNF, SnO_2 nanoflakes, and SnO_2 nanoparticles cells is shown in Figure 7a. After 100 cycles at 0.1 C, the SnO_2 nanoflakes/CNF cell retained a higher capacity of approximately 636 mAh g^{-1},

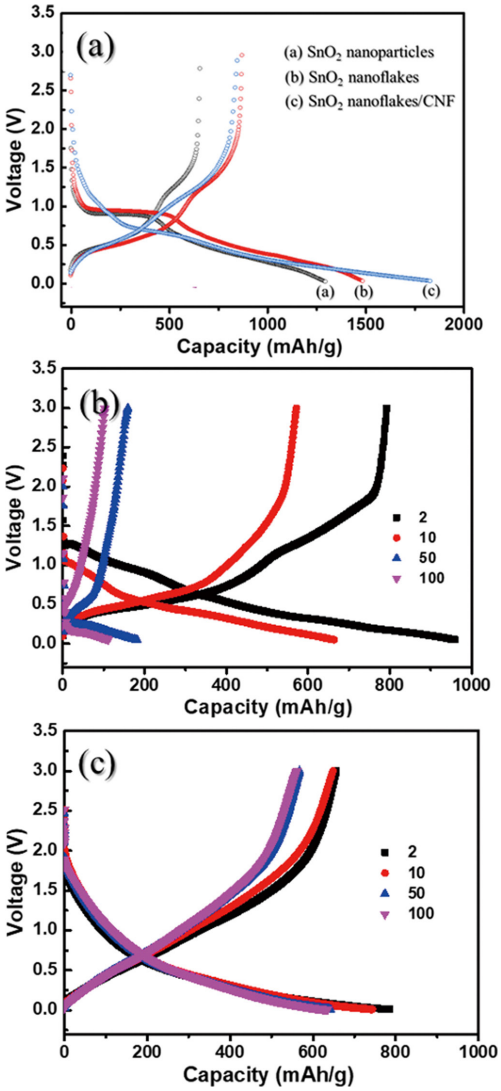

Figure 6. (a) initial charge–discharge profiles of SnO_2 nanoparticles, SnO_2 nanoflakes, and SnO_2 nanoflakes/CNF, subsequent charge-discharge profiles of (b) SnO_2 nanoflakes, (c) SnO_2 nanoflakes/CNF at 0.1 C.

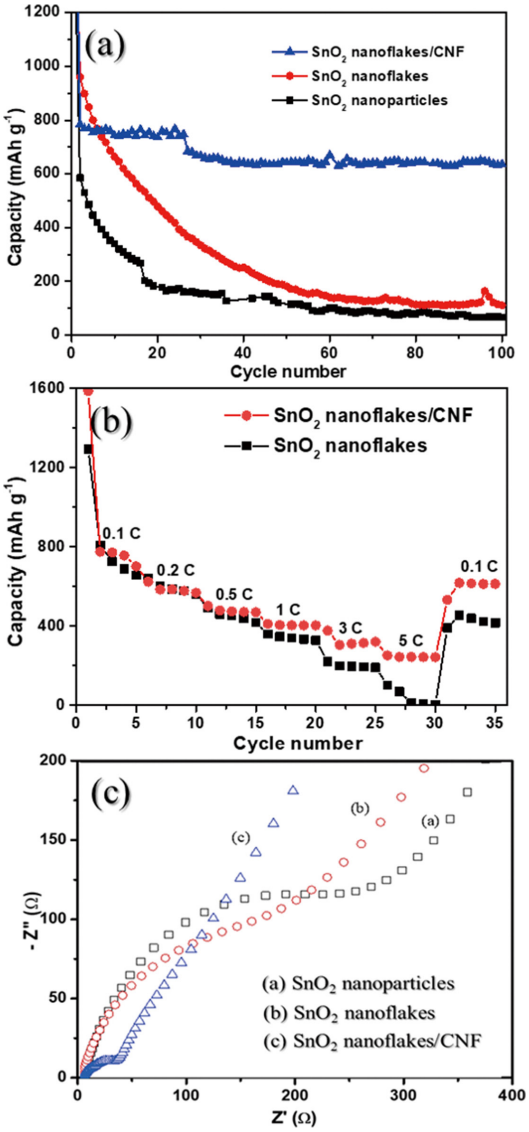

Figure 7. (a) cycling performances of SnO_2 nanoparticles, SnO_2 nanoflakes, and SnO_2 nanoflakes/CNF at 0.1 C, (b) rate performances of SnO_2 nanoflakes, and SnO_2 nanoflakes/CNF, and (c) EIS plots of SnO_2 nanoparticles, SnO_2 nanoflakes, and SnO_2 nanoflakes/CNF after 100 cycles.

corresponding to 81.1% of the capacity from the 2nd cycle. The electrochemical performance of SnO_2 nanoflakes/CNF exceeds the previously reported electrochemical performance of SnO_2/carbon composites, as shown in Table 1[30-34]. In contrast, the SnO_2 nanoflakes and SnO_2 nanoparticles cells exhibited significantly lower retained capacities of only 111 and 67 mAh g^{-1}, respectively,

Table 1. Summary of previous studies on SnO_2/carbon composite-based anode for LIBs

Anode material employed	Current density (mA g^{-1})	Initial lithiation capacity (mAh g^{-1})	Retained lithiation capacity (mAh g^{-1})	Cycles	Refs
Flexible SnO_2/G-CNT paper	100	990	387	50	30
SnO_2/G-CNT	100	1,050	502	50	31
SnO_2/G-CNT	200	1,806	842	40	32
SnO_2-G	50	2,140	649	30	33
SnO_2/gC	50	1,675	592	100	34
SnO_2/MWNT	50	907	231	50	
SnO_2 nanoflakes/CNF	0.1 C	1,800	636	100	This work

after 100 cycles. This highlights the significant improvement in the reversibility of the conversion reaction provided by the SnO_2 nanoflakes/CNF composite. Moreover, a rate capability test was conducted for the SnO_2 nanoflakes/CNF and SnO_2 nanoflakes cells, as shown in Figure 7b. The test began at 0.1 C for 5 cycles, progressively increased to 5 C, and then decreased back to 0.1 C. The SnO_2 nanoflakes/CNF cell achieved initial lithiation capacities of 1,587, 625, 503, 412, 378, 252, and 614 mAh g^{-1}, while the SnO_2 nanoflakes cell achieved 1,295, 641, 493, 360, 221, 102, and 417 mAh g^{-1} at 0.1, 0.2, 0.5, 1, 3, 5, and 0.1 C, respectively. The superior rate capability of the SnO_2 nanoflakes/CNF composite can be attributed to its unique hybrid structure, where the CNF enhances electrical conductivity and buffers volume changes during charge-discharge processes. Additionally, the *in-situ* generated SnO_2 nanoflakes shorten the ion transport path and increase the contact area between the active material and the electrolyte, thereby enhancing the electrochemical performance. Furthermore, the EIS spectra for SnO_2 nanoflakes/CNF, SnO_2 nanoflakes, and SnO_2 nanoparticles cells were obtained in the fully delithiated state after 100 cycles (Figure 7c). The Nyquist plots for these cells display a depressed semicircle in the high-middle frequency region, indicative of the charge transfer resistance (R_{ct}), and a sloped line in the low-frequency region, representing the Warburg impedance (R_w) associated with Li^+ ion diffusion[35,36]. The R_{ct} of the cycled cell with SnO_2 nanoflakes/CNF is the lowest at 53 Ω, compared to 379 Ω for the cycled cell with SnO_2 nanoflakes and 414 Ω for the cell with SnO_2 nanoparticles. This is evidenced by the smaller depressed semicircle in the Nyquist plot for the SnO_2 nanoflakes/CNF cell, indicating faster reaction kinetics. The CNF serves as a conductive matrix, significantly enhancing electrical conductivity and reducing resistance in the SnO_2 nanoflakes/CNF cell. The Warburg factor (σ) is calculated from the slope of the plot of the real part of resistance against the inverse square root of the angular frequency in the low-frequency range, using Equation (3):

$$D = \frac{R^2T^2}{2A^2n^2F^4C^2\sigma^2} \quad (3)$$

where R is the gas constant, T is the absolute temperature, A is the electrode surface area, F is the Faraday constant, and C is the molar concentration of Li ions in the active material. The lithium diffusion coefficient (D) for the cycled SnO_2 nanoflakes/CNF cell is calculated to be 4.3×10^{-11} cm^2 s^{-1}, confirming the rapid reaction kinetics in the SnO_2 nanoflakes/CNF cell.

4. Conclusions

A hierarchical SnO_2 nanoflakes/CNF composite was effectively synthesized using a simple incipient wetness method followed by annealing. The composite exhibits outstanding cycling performance and excellent rate capability, attributed to three key factors: (1) the CNF matrix prevents the agglomeration of *in-situ* grown SnO_2 nanoflakes, enhances electrical conductivity, accelerates electron transport, and mitigates volume changes; (2) the *in-situ* generated SnO_2 nanoflakes increase active sites, enhance electrolyte accessibility and shorten ion and electron transport pathways; and (3) the synergistic interaction between SnO_2 nanoflakes and CNF matrix optimizes charge storage and transfer processes, improving overall electrochemical performance. As a result, the SnO_2 nanoflakes/CNF composite demonstrates exceptional rate capability and excellent cycling stability. This research offers valuable insights into the design of anode materials for LIBs, aiding the advancement of high-performance energy storage systems.

Acknowledgements

This research was supported by 'regional innovation mega project' program through the Korea Innovation Foundation funded by Ministry of Science and ICT (Project Number: 2023-DD-UP-0026) and the National Research Foundation of Korea (NRF) grant funded by the Korea government (MSIT) (No. RS-2023-00217581).

References

1. Xia, Q., Ni, M., Chen, M., and Xia, H., "Low-temperature Synthesized Self-supported Single-crystalline $LiCoO_2$ Nanoflake Arrays as Advanced 3D Cathodes for Flexible Lithium-ion Batteries," *J. Mater. Chem. A*, **7**, 6187-6196 (2019).
2. Autthawong, T., Yodbunork, C., Ratsameetammajak, N., Namsar, O., Chimupala, Y., and Sarakonsri, T., "Enhanced Electrochemical Performance of $Sn(SnO_2)/TiO_2$(B) Nanocomposite Anode Materials with Ultrafast Charging and Stable Cycling for High-performance Lithium-ion Batteries," *ACS Appl. Energy Mater.*, **5**, 13829-13842 (2022).
3. Kim, Y. B. and Park, G. D., "Synthesis of Porous-structured (Ni, Co)Se_2-CNT Microsphere and Its Electrochemical Properties as Anode for Sodium-ion Batteries," *Clean Technol.*, **29**, 178-184 (2023).
4. Zhu, Y., Huang, Y., and Wang, M., "Three-dimensional Hierarchical Porous $MnCo_2O_4$@MnO_2 Network towards Highly Reversible Lithium Storage by Unique Structure," *Chem. Eng. J.*, **378**, 122207 (2019).
5. Sun, C. R. and Kim, J. H., "Development of Bismuth Alloy-based Anode Material for Lithium Ion Battery," *Clean Technol.*, **30**, 23-27 (2024).

6. Li, Q., Li, H., Xia, Q., Hu, Z., Zhu, Y., Yan, S., Ge, C., Zhang, Q., Wang, X., Shang, X., Fan, S., Long, Y., Gu, L., Miao, G., Yu, G., and Moodera, J. S., "Extra Storage Capacity in Transition Metal Oxide Lithium-ion Batteries Revealed by in situ Magnetometry," *Nat. Mater.*, **20**, 76-83 (2021).
7. Zhang, J. and Yu, A., "Nanostructured Transition Metal Oxides as Advanced Anodes for Lithium-ion Batteries," *Sci. Bull.*, **60**, 823-838 (2015).
8. Fang, S., Bresser, D., and Passerini, S., "Transition Metal Oxide Anodes for Electrochemical Energy Storage in Lithium- and Sodium-ion Batteries," *Adv. Energy Mater.*, **10**, 1902485 (2020).
9. Zhou, S., Zhou, H., Zhang, Y., Zhu, K., Zhai, Y., Wei, D., and Zeng, S., "SnO_2 Anchored in S and N co-doped Carbon as the Anode for Long-life Lithium-ion Batteries," *Nanomaterials*, **12**, 700 (2022).
10. Cheng, Y., Wang, S., Zhou, L., Chang, L., Liu, W., Yin, D., Yi, Z., and Wang, L., "SnO_2 Quantum Dots: Rational Design to Achieve Highly Reversible Conversion Reaction and Stable Capacities for Lithium and Sodium Storage," *Small*, **16**, 2000681 (2020).
11. Lu, Z., Kong, Z., Jing, L., Wang, T., Liu, X., Fu, A., Guo, P., Guo, Y., and Li, H., "Porous SnO_2/graphene Composites as Anode Materials for Lithium-ion Batteries: Morphology Control and Performance Improvement," *Energ. Fuel.*, **34**, 13126-13136 (2020).
12. Wang, X., Zheng, T., Cheng, Y., Yin, S., Xia, Y., Ji, Q., Xu, Z., Liang, S., Ma, L., Zuo, X., Meng, J., Zhu, J., and Müller-Buschbaum, P., "SnO_2/Sn/Carbon Nanohybrid Lithium-ion Battery Anode with High Reversible Capacity and Excellent Cyclic Stability," *Nano Select*, **2**, 642-653 (2021).
13. Zhang, Y., Li, D., Qin, L., Zhao, P., Liu, F., Chuai, X., Sun, P., Liang, X., Gao, Y., Sun, Y., and Lu, G., "Preparation and Gas Sensing Properties of Hierarchical Leaf-like SnO_2 Materials," *Sensor. Actuat. B-Chem.*, **255**, 2944-2951 (2018).
14. Madhu, S., Ramasamy, S., Magudeeswaran, V., Manickam, P., Nagamony, P., and Chinnuswamy, V., "SnO_2 Nanoflakes Deposited Carbon Yarn-based Electrochemical Immunosensor towards Cortisol Measurement," *J. Nanostructure Chem.*, **13**, 115-127 (2023).
15. Narsimulu, D., Naresh, N., Rao, B. N., and Satyanarayana, N., "Rational Design of SnO_2 Nanoflakes as a Stable and High Rate Anode for Lithium-ion Batteries," *J. Mater. Sci.-Mater. El.*, **31**, 8556-8563 (2020).
16. Park, J. S., Jo, J. H., Yashiro, H., Kim, S., Kim, S., Sun, Y., and Myung, S. T., "Synthesis and Electrochemical Reaction of Tin Oxalate-reduced Graphene Oxide Composite Anode for Rechargeable Lithium Batteries," *ACS Appl. Mater. Interf.*, **9**, 25941-25951 (2017).
17. Ambalkar, A. A., Panmand, R. P., Kawade, U. V., Sethi, Y. A., Naik, S. D., Kulkarni, M. V., Adhyapak, P. V., and Kale, B. B., "Facile Synthesis of SnO_2@carbon Nanocomposites for Lithium-ion Batteries," *New J. Chem.*, **44**, 3366-3374 (2020).
18. Ma, C., Jiang, J., Xu, T., Ji, H., Yang, Y., and Yang, G., "Freeze-drying-assisted Synthesis of Porous SnO_2/rGO Xerogels as Anode Materials for Highly Reversible Lithium/sodium Storage," *ChemElectroChem*, **5**, 2387-2394 (2018).
19. Cheng, Y., Huang, J., Qi, H., Cao, L., Luo, X., Li, J., Xu, Z., and Yang, J., "Controlling the Sn-C bonds Content in SnO_2@CNTs Composite to Form in situ Pulverized Structure for Enhanced Electrochemical Kinetics," *Nanoscale*, **9**, 18681-18689 (2017).
20. Jung, S. M., Kim, D. W., and Jung, H. Y., "Unconventional Capacity Iincrease Kinetics of a Chemically Engineered SnO_2 Aerogel Anode for Long-term Stable Lithium-ion Batteries," *J. Mater. Chem. A*, **8**, 8244-8254 (2020).
21. Sun, J., Xiao, L., Jiang, S., Li, G., Huang, Y., and Geng, J., "Fluorine-doped SnO_2@graphene Porous Composite for High Capacity Lithium-ion Batteries," *Chem. Mater.*, **27**, 4594-4603 (2015).
22. Cheng, Y., Xie, H., Yu, F., Zhang, J., Wang, Y., Luo, X., Shi, B., and Liu, B., "Facile Fabrication of Three-dimensional Porous Carbon Embedded with SnO_2 Nanoparticles as a High-performance Anode for Lithium-ion Battery," *Ionics*, **27**, 4143-4151 (2021).
23. Zhan, L., Zhou, X., Luo, J., and Ning, X., "Binder-free Multilayered SnO_2/graphene on Ni Foam as a High-performance Lithium Ion Batteries Anode," *Ceram. Int.*, **45**, 6931-6936 (2019).
24. Wang, M., Wang, X., Yao, Z., Tang, W., Xia, X., Gu, C., and Tu, J., "SnO_2 Nanoflake Arrays Coated with Polypyrrole on a Carbon Cloth as Flexible Anodes for Sodium-Ion Batteries," *ACS Appl. Mater. Interfaces*, **11**, 24198-24204 (2019).
25. Wang, Z., Chen, L., Feng, J., Liu, S., Wang, Y., Fan, Q., and Zhao, Y., "*In-situ* Grown SnO_2 Nanospheres on Reduced GO Nanosheets as Advanced Anodes for Lithium-ion Batteries," *ChemistryOpen*, **8**, 712-718 (2019).
26. Chen, J. S., Cheah, Y. L., Chen, Y. T., Jayaprakash, N., Madhavi, S., Yang, Y. H., and Lou, X. W., "SnO_2 Nanoparticles with Controlled Carbon Nanocoating as High-capacity Anode Materials for Lithium-ion Batteries," *J. Phys. Chem. C*, **113**, 20504-20508 (2009).
27. Tian, Z., Zhao, J., Li, B., Feng, Y., Song, J., Niu, C., Shao, L., and Zhang, W., "Controllable Synthesis of 3D Porous SnO_2/carbon towards Enhanced Lithium-ion Batteries," *Ionics*, **26**, 2773-2779 (2020).
28. Liang, J., Yu, X. Y., Zhou, H., Wu, H. B., Ding, S., and Lou, X. W., "Bowl-like SnO_2@carbon Hollow Particles as an Advanced Anode Material for Lithium-ion Batteries," *Angew. Chem. Int. Ed.*, **53**, 12803-12807 (2014).
29. Liu, M., Zhang, S., Dong, H., Chen, X., Gao, S., Sun, Y., Li, W., Xu, J., Chen, L., Yuan, A., and Lu, W., "Nano-SnO_2/carbon

Nanotube Hairball Composite as a High-capacity Anode Material for Lithium Ion Batteries," *ACS Sustainable Chem. Eng*., **7**, 4195-4203 (2019).

30. Zhang, B., Zheng, Q. B., Huang, Z. D., Oh, S. W., and Kim, J. K., "SnO_2-graphene-Carbon Nanotube Mixture for Anode Material with Improved Rate Capacities," *Carbon*, **49**, 4524-4534 (2011).
31. Chen, T., Pan, L., Liu, X., Yu, K., and Sun, Z., "One-step Synthesis of SnO_2-reduced Graphene Oxide-carbon Nanotube Composites via Microwave Assistance for Lithium Ion Batteries," *RSC Adv.*, **2**, 11719-11724 (2012).
32. Zhang, Z., Wang, L., Xiao, J., Xiao, F., and Wang, S., "One-pot Synthesis of Three-Dimensional Graphene/carbon Nanotube/ SnO_2 Hybrid Architectures with Enhanced Lithium Storage Properties," *ACS Appl. Mater. Interf.*, **7**, 17963-17968 (2015).
33. Zhu, X., Zhu, Y., Murali, S., Stoller, M. D., and Ruoff, R. S., "Reduced Graphene Oxide/tin Oxide Composite as an Enhanced Anode Material for Lithium Ion Batteries Prepared by Homogenous Coprecipitation," *J. Power Sources*, **196**, 6473-6477 (2011).
34. Sahoo, M. and Ramaprabhu, S., "Solar Synthesized Tin Oxide Nanoparticles Dispersed on Graphene Wrapped Carbon Nanotubes as a Li Ion Battery Anode Material with Improved Stability," *RSC Adv.*, **7**, 13789-13797 (2017).
35. Liu, Y., Li, X., Haridas, A. K., Sun, Y., Heo, J., Ahn, J. H., and Lee, Y., "Biomass-Derived Graphitic Carbon Encapsulated Fe/ Fe_3C Composite as an Anode Material for High-performance Lithium Ion Batteries," *Energies*, **13**, 827 (2020).
36. Liu, Y., Ju, H. C., Cho, K. K., Ahn, H. J., and Ahn, J. H., "Grape-cluster-like Hierarchical Structure of FeS_2 Encapsulated in Graphitic Carbon as Cathode Material for High-rate Lithium Batteries," *Appl. Surf. Sci*., **630**, 157458 (2023).